

ARTICLE

Open Access

Band anisotropy and effective mass renormalization in strained metallic VO₂ (101) thin films

A. D'Elia^{1,2}, V. Polewczyk^{3,7}, A. Y. Petrov³, G. Vinai³, L. Li⁴, C. W. Zou⁴, S. J. Rezvani^{3,5} and A. Marcelli^{1,2,6}

Abstract

We explore how strain impacts the band structure of metallic-phase VO₂ thin films deposited on TiO₂(101) substrates. Employing a combination of X-ray absorption linear dichroism and valence band measurements, we demonstrate that strain can alter the intrinsic band structure anisotropy of metallic VO₂. Our findings reveal that reducing the thickness of VO₂ films leads to a more isotropic band structure. This observation is further supported by an analysis of the electronic population redistribution in the $d_{||}-\pi^*$ bands, which affects the screening length and induces effective mass renormalization. Overall, our results underscore the potential of strain manipulation in tailoring the electronic structure uniformity of thin films, thereby expanding the scope for engineering VO₂ functionalities.

Introduction

Among vanadium oxides, VO₂ stands out for its metal insulator transition (MIT)¹ from a monoclinic insulating phase to a tetragonal metallic phase upon heating^{1–3} (with a transition temperature T_C of 340 K in bulk), making it an ideal candidate for technological implementation. The concomitant occurrence of an MIT and a structural phase transition (SPT) sparked discussion over the nature of the MIT itself^{4–8}. After decades of debate, the state-of-the-art dominant theoretical scenario is that of a cooperative orbital-assisted Mott–Peierls mechanism⁹. The MIT in VO₂ is interesting from a technological point of view because of its reversible 3–4 orders of magnitude resistivity jump across the transition^{10,11}. These features enable applications such as smart windows and the development of new technologies spanning from neuro-morphic devices to memristive devices^{12–16}. In addition, the metallic phase of VO₂ has multiband characteristics and is intrinsically anisotropic. The electronic structure and thus the resistive properties strongly depend on the

crystal orientation^{17–21}. This is an often overlooked aspect that may lead to new appealing applications, such as efficient ion migration and coupling in synaptic devices²², nanoactuators²³ and the fabrication of dynamically reconfigurable optical elements²⁴. The ability to control VO₂ properties and, in particular, the electronic structure anisotropy is therefore of utmost importance to envision such implementations.

To understand the role of band anisotropy in the MIT properties, probing its electronic character close to the Fermi level (FL) in proximity to the phase transition is necessary. The high-temperature metallic phase of bulk VO₂ has lattice tetragonal symmetry (often called rutile and indicated with R). In this phase, two bands populate the FL, $d_{||}-\pi^*$. $d_{||}$ is directed along the c axis (c_r) and is composed of the superposition of a_{1g} orbitals². The π^* band is formed by the antibonding band generated by the chemical bond between vanadium e_g^π and O 2p electrons and is directed in the a_r-b_r plane, i.e., perpendicular to the $d_{||}$ band. When the temperature decreases, a combination of structural distortion and electron correlation takes place, resulting in dimerization of the V atoms along the c_r axis. This leads to an increased overlap of the a_{1g} orbitals that split the $d_{||}$ band into the empty $d_{||}^*$ band and the populated $d_{||}$ band. The structural distortion also increases the energy of the π^* band². The combination of

Correspondence: A. D'Elia (alessandro.delia@lnf.infn.it)

¹Istituto Nazionale di Fisica Nucleare, Laboratori Nazionali di Frascati, 00044 Frascati, Italy

²CNR - Istituto Struttura della Materia, Basovizza Area Science Park, Trieste 34149, Italy

Full list of author information is available at the end of the article

© The Author(s) 2024



Open Access This article is licensed under a Creative Commons Attribution 4.0 International License, which permits use, sharing, adaptation, distribution and reproduction in any medium or format, as long as you give appropriate credit to the original author(s) and the source, provide a link to the Creative Commons licence, and indicate if changes were made. The images or other third party material in this article are included in the article's Creative Commons licence, unless indicated otherwise in a credit line to the material. If material is not included in the article's Creative Commons licence and your intended use is not permitted by statutory regulation or exceeds the permitted use, you will need to obtain permission directly from the copyright holder. To view a copy of this licence, visit <http://creativecommons.org/licenses/by/4.0/>.

these two events opens a band gap, ultimately transforming the metallic tetragonal VO₂ into a monoclinic insulator.

In recent years, strain modification has emerged as one of the most successful methods for manipulating complex oxide electronic structures^{25–29}. In VO₂, the MIT is modified by strain since it alters the interatomic distances; hence, the orbitals overlap, with consequences for the transition properties. The two most studied cases are those where tensile or compressive strains on the *c_r* axis are applied through epitaxial growth of VO₂ thin films by tuning the lattice mismatch as a function of the chosen substrate. Multiple studies have reported the MIT properties of VO₂ films grown along the (110), (100) and (001) surfaces of TiO₂^{11,30–35}. The *c_r* axis is oriented parallel (110 and 100 orientations) or perpendicular (001 orientation) to the film surface. Since the lattice parameters of TiO₂ are greater than those of VO₂, compressive out-of-plane strain and in-plane tensile strain occur. In VO₂ films oriented along the (110) and (100) planes, the critical temperature is higher than that in the bulk^{36,37}, and the severe in-plane tensile strain applied to the *c_r* axis allows the emergence of metastable phases^{31,38}. However, for this reason, the MIT of these films is usually quite broad^{35,36}, which hinders their potential for various applications. On the other hand, VO₂ films oriented along the (001) direction experience compressive strain in the *c_r* axis. The transition of these materials is quite sharp (which is favorable for producing devices with high ON-OFF ratios), whereas the critical temperature is lower than that of the bulk material (as low as 295 K)³³. The suppressed critical temperature may be unfavorable for devices operating at room temperature. Moreover, the high surface energy may result in undesired surface roughening, hindering the integration of these films in complex electronics^{39–41}. The (001), (110) and (100) VO₂ film orientations have been the most studied since they heavily strain (compressive or tensile) the *c_r* axis.

An intermediate case is that of VO₂ films grown on the TiO₂ (101) surface. For this orientation, the lattice mismatch is small, resulting in a reduced strain on the *c_r* axis that it is oriented diagonally out of plane^{37,41}. Compared with the other cases, these films combine sharp bulk-like MITs, as in the case of films those grown along the (001) direction, with approximately room-temperature T_cs and atomically smooth surfaces, which is ideal for implementation into heterostructures^{34,35,41}. In addition, an intermediate strain configuration is likely to minimize crack formation and self-pixelation on the film surface because the elastic stress is relieved across the MIT^{42–44}, increasing the stability of the transition. However, a detailed study of the band structure of VO₂ (101) as a function of strain is, to the best of our knowledge, still

lacking. In particular, the effect of moderate strain on band structure anisotropy has yet to be explored.

In this framework, we investigated the role of strain as a control parameter for the band structure anisotropy of VO₂ single-crystal films. Strain modulation was achieved by using VO₂ thin films of 8, 16 and 32 nm thickness on TiO₂ (101) substrates. The use of TiO₂ (101) is relatively less studied and hence still largely unexplored, and it is expected to apply an intermediate amount of strain along the *c_r* axis compared with that of TiO₂ (001)- and (110)-oriented films^{34,35}. The thin films set was characterized via X-ray diffraction (XRD) and resistivity measurements to determine the dependence of the film thickness on the MIT and the effect of substrate-induced strain on the lattice, respectively. The electronic structure evolution was then probed via X-ray absorption spectroscopy (XAS) and X-ray linear dichroism (XLD) at the V L₃ edge and resonant photoemission spectroscopy (ResPES). These measurements were performed using linearly polarized light to maximize *d*_{||}- and π^* -band sensitivity. The combined use of XLD and ResPES provides a complete overview of the band-selective projections of the unoccupied and occupied density of states of VO₂.

Our results revealed a progressive reduction in the anisotropy of the electronic structure of the VO₂/TiO₂(101) films as the thickness decreased; this is accompanied by an effective mass renormalization tending toward a scenario where *d*_{||} and π^* become increasingly similar as the film thickness decreases. These results highlight the key role of strain as a control parameter and the deep interconnection among band occupation, band curvature and anisotropy, which can be exploited for technological purposes.

Experimental

All the measurements were performed at 355 K except where specified otherwise. The VO₂/TiO₂(101) films were grown with an RF-plasma assisted oxide–molecular beam epitaxy (MBE) instrument at the University of Science and Technology of China, Hefei. The deposition chamber had a base pressure of less than 4×10^{-9} mbar. The substrate temperature was 823 K during deposition.

The synthesized thin films were characterized using XRD and resistivity measurements.

XRD measurements, both symmetric θ – 2θ scans and asymmetric reciprocal space maps, were performed using a PanAnalytical X'Pert Pro diffractometer (Cu–K α wavelength).

The T_cs of the MITs for all the samples were evaluated through transport measurements using the van der Pauw method.

The spectroscopy measurements were performed at the NFFA APE-HE beamline at the Elettra synchrotron radiation facility⁴⁵. XAS measurements were performed in

total electron yield (TEY) mode at the V L₃ edge while increasing the temperature from RT to 370 K via horizontal polarization. XLD measurements were obtained as the difference between the XAS spectra of the sample surface in different orientations with respect to the beam, as shown below. ResPES measurements were taken with a ScientaOmicron R3000 hemispherical analyzer, in which the photon energy across the V L₃ edge was scanned in horizontal polarization with the sample surface normal with respect to the analyzer. The binding energies were calibrated with respect to the Fermi level of a gold reference foil.

The (101) surface of the metallic VO₂ phase has [010] and [−101] vectors as in-plane lattice vectors. The a_r [100] and c_r [001] axes are inclined with respect to the normal to the surface with angles β ≈ 58° and γ ≈ 32° (values calculated using the data reported in JCPDS no. 76-0675). The sample surface was rotated by an angle of α = +45° or −45° with respect to the beam to align the electric field vector of the photon beam (\vec{E}) in a parallel orientation with respect to either c_r or a_r (i.e., perpendicular to c_r), as shown in the sketch of Fig. 1. This configuration creates an effective angle between \vec{E} and c_r (a_r) of δ ≈ 13°. This small angle does not significantly affect our data since both the absorption and photoemission intensities depend on cos²(δ)⁴⁶, which in this case corresponds to ≈ 0.95 ensuring that the orbital polarization of our data is 95%. Polarization-dependent measurements with similar values of δ have been successfully carried out in the literature⁴⁷.

By setting the electric field to be aligned parallel (E || c_r) or perpendicular (E ⊥ c_r, i.e., E || a_r) to c_r, it is possible to probe the empty d_{||} and π* bands, respectively⁴⁸.

Linear dichroism provides information on the evolution of the empty states relative to a specific band as a function of the film thickness. The XLD is calculated as follows:

$$XLD = 100 \times \frac{I_{||} - I_{\perp}}{I_{||} + I_{\perp}} \quad (1)$$

where I_{||} is the integrated intensity of the XAS acquired with E || c_r and I_⊥ is that of the XAS acquired with E ⊥ c_r. In this form, Eq. (1) can be used to determine the percentage of empty states in d_{||} with respect to those in the π* band.

Results and discussion

Resistivity

The resistivity measurements as a function of temperature for the entire set of films are reported in Fig. 1c.

All the resistivity curves exhibit a variation of approximately 3 orders of magnitude across the MIT, confirming the good quality of the films for all thicknesses. The critical temperature T_C (calculated as the average

temperature position between the two minima of $\frac{\partial \log \rho}{\partial T}$) and the transition width ΔT are reported in Table 1.

The data show that the T_C slightly increased by ~4 K when the film thickness was reduced. This agrees well with other studies reporting the temperature trend of VO₂/TiO₂(101) films⁴¹ and with what was observed for the twin VO₂/TiO₂(011) orientation³⁴. On the other hand, the transition width (ΔT) roughly doubles from 32 to 8 nm in thickness, indicating that strain reduces the lattice compatibility between the insulating and metallic phases of VO₂/TiO₂(101)⁴⁹.

XRD

For all the films, the diffraction pattern shows the presence of a single-crystal phase. The θ – 2θ scans of the 32 nm film of both the metallic and insulator phases are reported in Fig. 1d. The presence of Laue fringes indicates a sharp VO₂/TiO₂ interface. To calculate the a_r and c_r lattice parameters of metallic VO₂, we measured the reciprocal space map (RSM) of the (301) peak (shown in Fig. 1f, right panel). The calculated a_r and c_r are 4.556 and 2.834 Å, respectively. Compared with the reference value for tetragonal (metallic) VO₂ reported in JCPDS no. 76-0675, we observe a shortening of the c_r axis by approximately 0.7%, whereas the a_r axis remains mostly unchanged. The signal from the (301) reflection of the 16 and 8 nm films was below our detection threshold; thus, we could not measure the changes in their a_r and c_r axes. The (101) reflection of the metallic phase for the 8, 16 and 32 nm films is shown in Fig. 1e. The increase in the full width at the half maximum of the (101) peak agrees with the reduced thickness of the films and with what has been reported in the literature^{41,50,51}.

XAS and ResPES

To study the change in the electronic structure of metallic VO₂ as a function of the film thickness, we performed XLD and ResPES measurements at the V L₃ edge of the VO₂/TiO₂(101) films. The effect of compressive strain along c_r on the band structure involves transferring part of the electron population of the d_{||} band to the π* band^{2,11,30,47,52,53}. This population transfer is more pronounced for thinner films since the strain increases.

The linearly polarized XAS spectra and the calculated dichroism measured at 350 K are reported in Fig. 2a, b.

Clear spectroscopic differences are observable in the XAS spectra for the two different orientations. The dichroic percentage as a function of the film thickness, calculated according to Eq. (1), is reported in Fig. 2b. The dichroic percentage decreases as the film thickness increases, a trend that is in very good agreement with similar quantifications of the d_{||} – π* linear dichroism⁴⁷; this means that by reducing the film thickness, the empty states of d_{||} increase with respect to that of the π* band. In

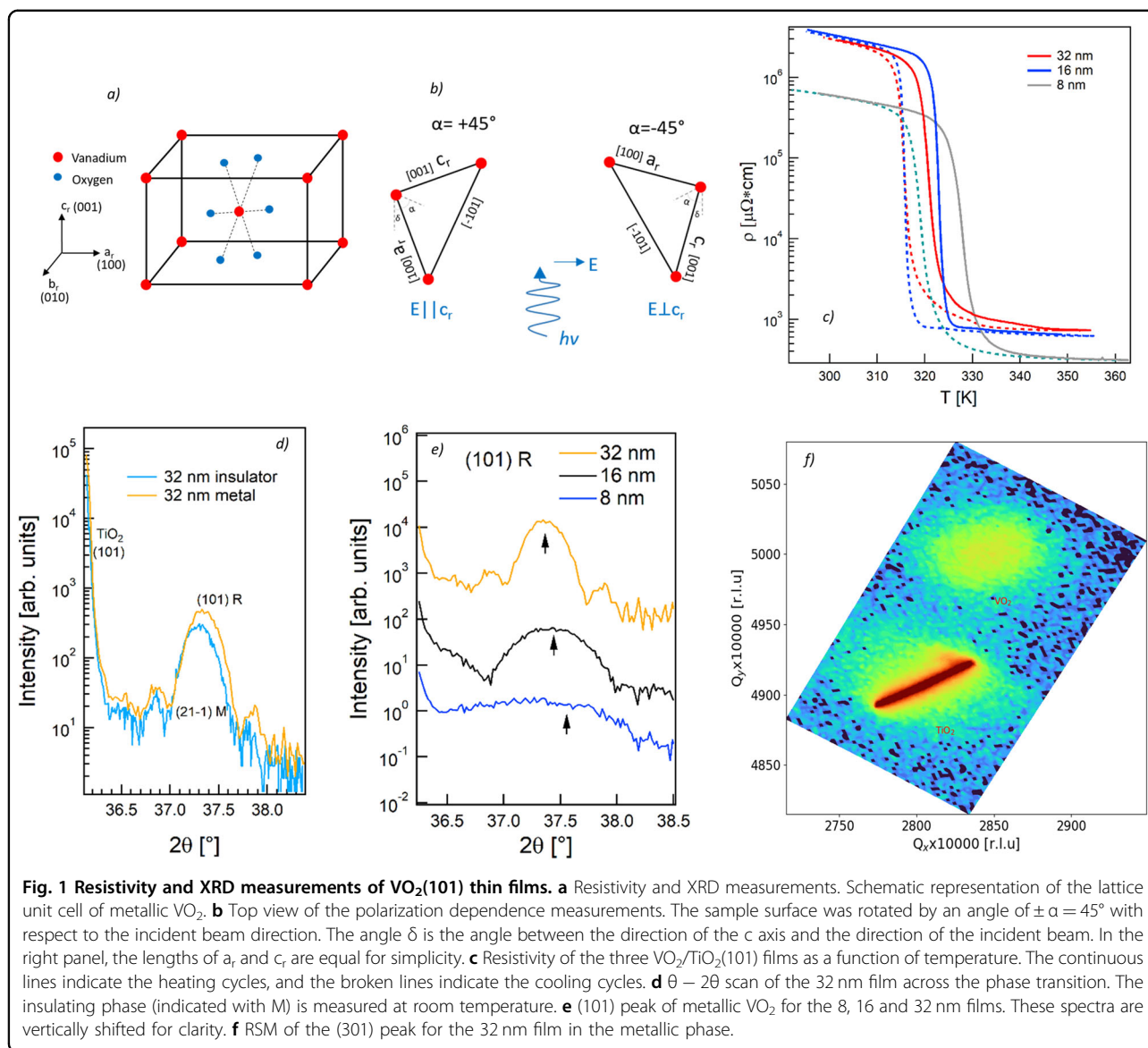


Table 1 Critical temperatures T_c and transition widths ΔT as a function of the film thickness.

Thickness [nm]	T_c [K]	ΔT [K]
8	321	8.2
16	318.4	6.8
32	316.8	4.3

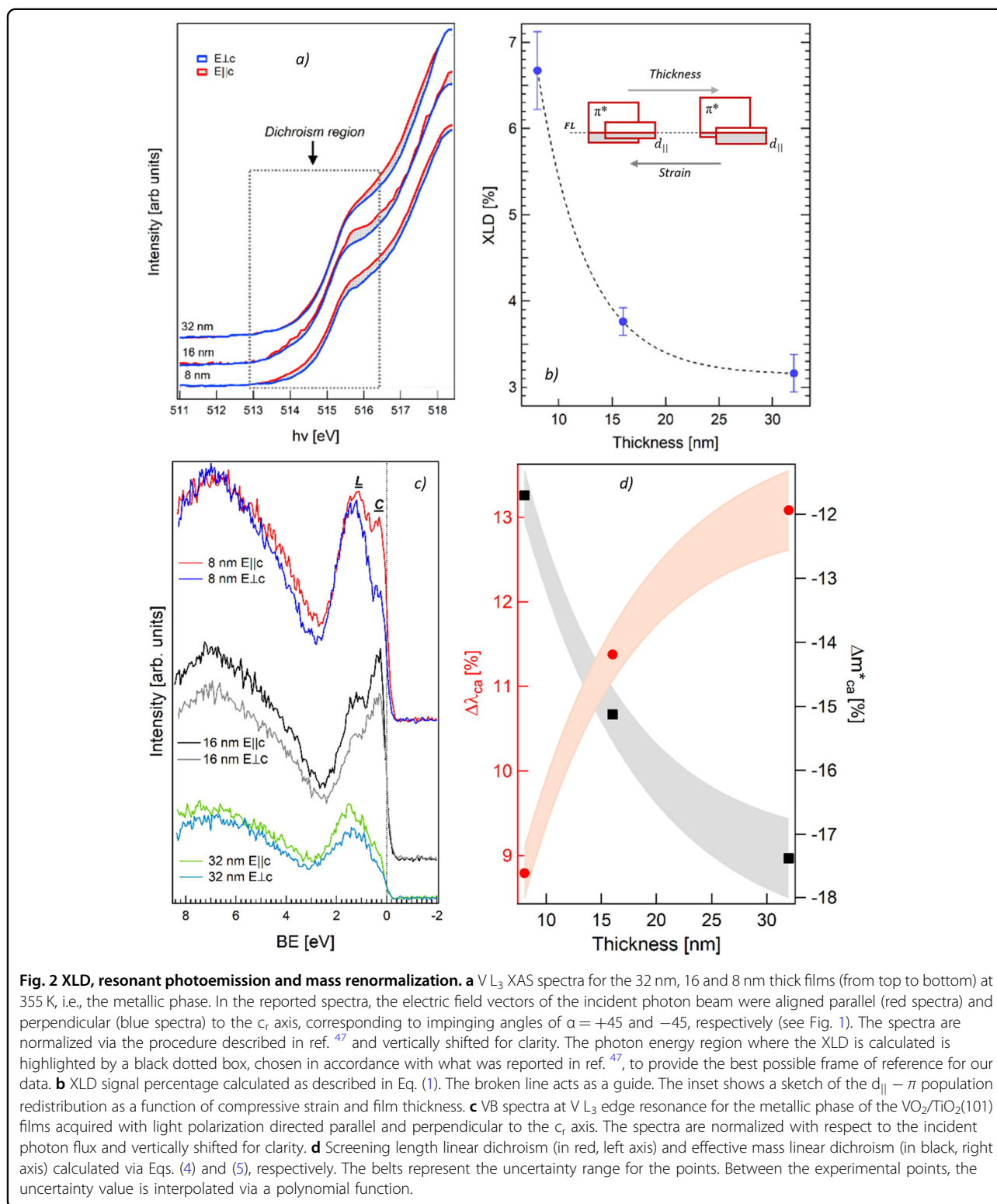
other words, the $d_{||}$ electron population decreases as π^* increases. These measurements demonstrate the $d_{||}-\pi^*$ band population transfer for VO₂/TiO₂(101) films.

To investigate the effect of the population redistribution of the $d_{||}$ and π^* bands on the electronic structure of VO₂ thin films, we performed linearly polarized photoemission

measurements at the V L₃ edge in resonance. This technique increases the sensitivity of the bands to the photoelectron spectra and, at the same time, maximizes the photoelectron yield. In particular, when $E || c_r$, the dipole matrix element of the V 3d photoemission spectra maximize the contribution from the $d_{||}$ orbital, whereas for $E \perp c_r$, it maximizes the π^* orbital⁵⁴; this is particularly relevant in proximity to the FL since electron population redistribution occurs in this energy region.

We studied the VB spectra of the 8, 16, and 32 nm samples in the $-2; 8$ eV binding energy (BE) region collected at the maximum V L₃ (518.4 ± 0.1 eV) resonance with $E || c_r$ and $E \perp c_r$.

The spectra are reported in Fig. 2c and are in good agreement with previous ResPES measurements reported in the literature for the same compound^{53,55–58}. Two



main features are observable. The peak centered at approximately 6 eV is due to hybridization between V 3d and O 2p electrons, whereas the feature that crosses the FL is generated by unpaired 3d electrons. The \underline{L} (ligand

hole) and \underline{C} (coherent hole) features are centered at BEs of approximately 1.7 and 0.5 eV, respectively^{53,56,59} for all the samples and for both orientations. The intensity of the \underline{L} and \underline{C} contributions changes as a function of the

polarization, mirroring the band orientation in the samples. The \underline{C} feature is less intense than the \underline{L} feature for the 8 and 32 nm samples, whereas the opposite is true for the 16 nm sample; this may be due to surface contamination of the samples since the measurements were performed *ex situ*. Nonetheless, this does not influence our analysis for three main reasons: a) the photon energy is set at the VO₂ V L₃ resonance; therefore, the contributions from other undesired vanadium oxides (such as V₂O₅ or V₂O₃) are damped[4]; b) at 355 K, VO₂ is the only metallic oxide contributing to the valence band close to the FL (except for V₆O₁₃⁶⁰, which is not observed at low temperature and can thus be ruled out; and c) the orientation-dependent intensity variations of the VB at the V L₃ edge are due to the orbital anisotropy of VO₂ since spurious oxides are expected to contribute isotropically to the photoemission intensity.

We used linearly polarized ResPES to probe the dichroism in the metallicity (i.e., the ability to screen an electric field) induced by the change in the band population^{61–63}. The maximum intensity (normalized with respect to the photon flux) of the resonant photoemission feature can be linked to the screening length via Eq. (2)^{61–63}

$$\frac{I}{I_0} \propto \lambda \quad (2)$$

where I is the VB peak integral intensity, I_0 is the incident photon flux and λ is the screening length. Owing to the orbital sensitivity of the measurements, the variation in the screening length $\Delta\lambda$ along the c_r axis and along the a_r axis is calculated as follows:

$$\Delta\lambda_{ca} = 100 \times \frac{I_c - I_a}{I_c + I_a} \propto 100 \times \frac{\lambda_c - \lambda_a}{\lambda_c + \lambda_a} \quad (3)$$

where $\Delta\lambda_{ca}$ is expressed as a percentage; I_c and I_a are the normalized integrated intensities of the VB spectra acquired with $E_{||}$ c_r and $E_{\perp c_r}$, respectively; and λ_c and λ_a are the screening lengths due to the $d_{||}$ and π^* bands, respectively. To calculate $\Delta\lambda_{ca}$, we integrated the intensity of the VB spectra in the binding energy region of 0–2 eV to include both \underline{L} and \underline{C} contributions. The data are represented as red dots in Fig. 2d.

$\Delta\lambda_{ca}$ increases as the film thickness increases, indicating that the screening capability of VO₂ decreases as the film thickness decreases. The anisotropy reduction also affects the effective masses of the $d_{||}$ and π^* bands. The screening length can be expressed in a general form as follows⁶⁴:

$$\lambda^{-2} = \frac{\sqrt{2}e^2 m^{*\frac{3}{2}} (k_b T)^{\frac{1}{2}}}{2\pi\epsilon_0 \hbar^3} F'_{\frac{1}{2}}\left(\frac{\mu}{k_b T}\right) \quad (4)$$

where e is the electron charge, m^* is the effective mass, $k_b T$ is the temperature multiplied by the Boltzman

constant, \hbar is the reduced Plank constant, ϵ_0 is the vacuum permeability, and $F'_{1/2}(\mu/(k_b T))$ is the first derivative of the Fermi integral of order $\frac{1}{2}$ with respect to $\mu/(k_b T)$, where μ is the chemical potential⁶⁵. $F'_{1/2}(\mu/(k_b T))$ depends on the temperature and the relative position of the conduction band edge with respect to the FL.

In our case, since the polarized ResPES were acquired at the same temperature and since the chemical potential within the same sample remains the same, from Eq. (4), we obtain

$$\Delta m_{ca}^* = \frac{m_c^* - m_a^*}{m_c^* + m_a^*} = \frac{\lambda_c^{-\frac{4}{3}} - \lambda_a^{-\frac{4}{3}}}{\lambda_c^{-\frac{4}{3}} + \lambda_a^{-\frac{4}{3}}} \quad (5)$$

where Δm_{ca}^* is the difference between the effective masses m_c^* and m_a^* . The calculated Δm_{ca}^* values are reported in Fig. 2d as black squares. The trend is the same as that of $\Delta\lambda_{ca}$, where the dichroism decreases (in absolute value) with decreasing film thickness. Our results agree well with the effective mass difference calculated via the angle-resolved photoemission data reported in⁶⁶, for which $\Delta m_{ca}^* \approx 18 - 20\%$ for a 20 nm thick VO₂ film. By reducing the film thickness, we observe an effective mass renormalization, pointing toward a reduction in the anisotropy in the band structure.

We can summarize our observations as follows: the strain-induced electronic population redistribution between $d_{||}$ and π^* leads to increased homogeneity of the screening length and the effective mass along the a_r and c_r axes.

Our observations agree with the results of the LDA and DFT calculations for strained VO₂ films with a shortened c_r axis^{67,68}. The reduction in the V–V pair distance increases the overlap of the a_{1g} ($d_{||}$) orbitals, leading to renormalization of the bandwidth. This renormalization generally results in different occupation numbers in different orbitals, i.e., in charge transfer between the $d_{||}$ and π^* bands. In the case of a shortened c_r axis, this results in an increase in the a_{1g} – a_{1g} hopping terms and an increase in the corresponding bandwidth⁶⁷. This ultimately reduces the energy difference between the $d_{||}$ and π^* bands, leading to a more even population of the two bands, which weakens the repulsive electron–electron interaction⁶⁸. Our data confirm the prediction of an emerging isotropization of the band structure of VO₂ films driven by strain, which acts as a parameter that control the Mott physics in multiband complex oxides.

Conclusions

The role of strain in the modulation of band structure anisotropy in metallic VO₂/TiO₂(101) was investigated by combining XLD and ResPES. Our single-crystal films show compressive strain along the c_r axis, which leads to an electronic population redistribution between the $d_{||}$ and π^* bands, with the two bands more evenly populated

for thinner (strained) films. This leads to a decrease in the difference in screening length calculated along c_r and a_r as a function of film thickness, indicating a reduction in the anisotropy in the band structure of VO₂. This is further confirmed by the observation of an effective mass renormalization effect, which suggests that, in addition to the redistribution between the $d_{||}$ and π^* bands, the band curvature itself is also influenced by strain.

In other words, in the presence of interfacial strain along the (101) direction of the metallic phase, $d_{||}$ and π^* become similar in terms of the electron population, electric field screening performance and effective mass. Strain emerges as a dominant parameter controlling the Mott physics of multiband oxides, allowing for the tuning of the anisotropy of the VO₂ band structure. Our results shed light on the band structure properties of these poorly investigated strained VO₂(101) thin films, whose properties are promising for technological applications based on intrinsic anisotropy of materials.

Acknowledgements

This work was partially performed in the framework of the Nanoscience Foundry and Fine Analysis (NFFA-MUR Italy Progetti Internazionali) facility (<https://www.trieste.nffa.eu/>).

Author details

¹Istituto Nazionale di Fisica Nucleare, Laboratori Nazionali di Frascati, 00044 Frascati, Italy. ²CNR - Istituto Struttura della Materia, Basovizza Area Science Park, Trieste 34149, Italy. ³CNR - Istituto Officina dei Materiali (IOM), Area Science Park, S.S.14, km 163.5, I-34149 Trieste, Italy. ⁴National Synchrotron Radiation Laboratory, University of Science and Technology of China, Hefei 230029, PR China. ⁵Scuola di Scienze e Tecnologie, Sezione di Fisica, Università di Camerino, Via Madonna delle Carceri 9, 62032 Camerino, Italy. ⁶Rome International Center for Materials Science Superstripes RICMASS, Via dei Sabelli 119A, Roma 00185, Italy. ⁷Present address: Université Paris-Saclay, UVSQ, CNRS, GEMaC, 78000 Versailles, France

Author contributions

A.D. conceived the experiment; G.V., V.P., A.P. performed the measurements, L.L., C.Z. synthesized the samples; A.D., J.R., data analysis; A.D. original manuscript writing; A.D., V.P., G.V., A.P., C.Z., L.L., J.R., A.M., reviewed and revised the manuscript; all the authors reviewed and approved the final version of the manuscript.

Competing interests

The authors declare no competing interests.

Publisher's note

Springer Nature remains neutral with regard to jurisdictional claims in published maps and institutional affiliations.

Supplementary information The online version contains supplementary material available at <https://doi.org/10.1038/s41427-024-00576-2>.

Received: 24 January 2024 Revised: 20 September 2024 Accepted: 14 October 2024

Published online: 22 November 2024

References

- Morin, F. J. Oxides which show a metal-to-insulator transition at the neel temperature. *Phys. Rev. Lett.* **3**, 34–36 (1959).

- Goodenough, J. B. The two components of the crystallographic transition in VO₂. *J. Solid State Chem.* **3**, 490–500 (1971).
- Narayan, J. & Bhosle, V. M. Phase transition and critical issues in structure-property correlations of vanadium oxide. *J. Appl. Phys.* **100**, 103524 (2006).
- Zimmermann, R., Claessen, R., Reinert, F., Steiner, P. & Hüfner, S. Strong hybridization in vanadium oxides: evidence from photoemission and absorption spectroscopy. *J. Phys. Condens. Matter* **10**, 5697–5716 (1998).
- Qazilbash, M. M. et al. Correlated metallic state of vanadium dioxide. *Phys. Rev. B Condens. Matter. Mater. Phys.* **74**, 205118 (2006).
- Weber, C. et al. Vanadium dioxide: A Peierls-Mott insulator stable against disorder. *Phys. Rev. Lett.* **108**, 256402 (2012).
- Zylbersztein, A. & Mott, N. F. Metal-insulator transition in vanadium dioxide. *Phys. Rev. B* **11**, 4383–4395 (1975).
- Eyert, V. The metal-insulator transitions of VO₂: A band theoretical approach. *Ann. Der Phys.* **11**, 650–704 (2002).
- Grandi, F., Amaricci, A. & Fabrizio, M. Unraveling the Mott-Peierls intrigue in vanadium dioxide. *Phys. Rev. Res.* **2**, 013298 (2020).
- Fu, D. et al. Comprehensive study of the metal-insulator transition in pulsed laser deposited epitaxial VO₂ thin films. *J. Appl. Phys.* **113**, 043707 (2013).
- Fan, L. L. et al. Strain dynamics of ultrathin VO₂ film grown on TiO₂ (001) and the associated phase transition modulation. *Nano Lett* **14**, 4036–4043 (2014).
- Chen, S. et al. Gate-controlled VO₂ phase transition for high-performance smart windows. *Sci. Adv.* **5**, eaav6815 (2019).
- Corti, E. et al. Scaled resistively-coupled VO₂ oscillators for neuromorphic computing. *Solid State Electron* **168**, 107729 (2020).
- Brahlek, M. et al. D. G. Opportunities in vanadium-based strongly correlated electron systems. *MRS Commun* **7**, 27–52 (2017).
- Samizadeh Nikoo, M. et al. Electrical control of glass-like dynamics in vanadium dioxide for data storage and processing. *Nat. Electron.* **5**, 596–603 (2022).
- Corti, E. et al. Coupled VO₂ Oscillators Circuit as Analog First Layer Filter in Convolutional Neural Networks. *Front. Neurosci.* **15**, 1–12 (2021).
- Kittiwatanakul, S., Lu, J. & Wolf, S. A. Transport Anisotropy of Epitaxial VO₂ Films near the Metal-Semiconductor Transition. *Appl. Phys. Express* **4**, 091104 (2011).
- Lu, J., West, K. G. & Wolf, S. A. Very large anisotropy in the dc conductivity of epitaxial VO₂ thin films grown on (011) rutile TiO₂ substrates. *Appl. Phys. Lett.* **93**, 1–4 (2008).
- Lee, S. et al. Anomalously low electronic thermal conductivity in metallic vanadium dioxide. *Science* **355**, 371–374 (2017).
- Bongers, P. F. Anisotropy of the electrical conductivity of VO₂ single crystals. *Solid State Commun* **3**, 275–277 (1965).
- Macis, S. et al. Anisotropic Optical Response of Ti-Doped VO₂ Single Crystals. *Materials* **17**, 3121 (2024).
- Park, J., Oh, C. & Son, J. Anisotropic ionic transport-controlled synaptic weight update by protonation in a VO₂ transistor. *J. Mater. Chem. C Mater.* **9**, 2521–2529 (2021).
- Manca, N. et al. Anisotropic Temperature-Driven Strain Dynamics in VO₂ Solid-State Microactuators. *ACS Appl Electron Mater* **3**, 211–218 (2021).
- John, J. et al. Tunable optical anisotropy in epitaxial phase-change VO₂ thin films. *Nanophotonics* **11**, 3913–3922 (2022).
- Poccia, N., Ricci, A. & Bianconi, A. Misfit strain in superlattices controlling the electron-lattice interaction via microstrain in active layers. *Adv. Condensed Matter Phys* **2010**, 261849 (2010).
- Poccia, N. et al. Optimum inhomogeneity of local lattice distortions in La₂CuO_{4+y}. *Proc. Natl Acad. Sci. USA* **109**, 15685–15690 (2012).
- Poccia, N. & Fratini, M. The misfit strain critical point in the 3D phase diagrams of cuprates. *J. Supercond. Nov. Magn.* **22**, 299–303 (2009).
- Ricci, A., Poccia, N., Ciasca, G., Fratini, M. & Bianconi, A. The microstrain-doping phase diagram of the iron pnictides: Heterostructures at atomic limit. *J. Supercond. Nov. Magn.* **22**, 589–593 (2009).
- Kugel, K. I., Rakhmanov, A. L., Sboychakov, A. O., Poccia, N. & Bianconi, A. Model for phase separation controlled by doping and the internal chemical pressure in different cuprate superconductors. *Phys. Rev. B Condens Matter Mater. Phys.* **78**, 1–7 (2008).
- Fan, L. L. et al. Comprehensive studies of interfacial strain and oxygen vacancy on metal-insulator transition of VO₂ film. *J. Phys.: Condens. Matter* **28**, 255002 (2016).
- Quackenbush, N. F. et al. Stability of the M₂ phase of vanadium dioxide induced by coherent epitaxial strain. *Phys. Rev. B* **94**, 085105 (2016).
- Evlukhin, E. et al. Directly measuring the structural transition pathways of strain-engineered VO₂ thin films. *Nanoscale* **12**, 18857–18863 (2020).

33. Quackenbush, N. F. et al. Nature of the metal insulator transition in ultrathin epitaxial vanadium dioxide. *Nano Lett* **13**, 4857–4861 (2013).
34. Kittiwatanakul, S., Wolf, S. A. & Lu, J. Large epitaxial bi-axial strain induces a Mott-like phase transition in VO₂. *Appl. Phys. Lett.* **105**, 073112 (2014).
35. Hong, B. et al. Strain engineering on the metal-insulator transition of VO₂/TiO₂ epitaxial films dependent on the strain state of vanadium dimers. *Appl. Phys. Lett.* **115**, 251605 (2019).
36. Jeong, J. et al. Suppression of metal-insulator transition in VO₂ by electric field-induced oxygen vacancy formation. *Science* **339**, 1402–1405 (2013).
37. Li, J. & Dho, J. Characteristics of phase transition of VO₂ films grown on TiO₂ substrates with different crystal orientations. *J. Cryst. Growth* **404**, 84–88 (2014).
38. Singh, C. N., Piper, L. F. J., Paik, H., Schlom, D. G. & Lee, W.-C. Correlation-induced emergent charge order in metallic vanadium dioxide. *Phys. Rev. B* **035150** (2022).
39. Ramamoorthy, M., Vanderbilt, D. & King-Smith, R. D. First-principles calculations of the energetics of stoichiometric TiO₂ surfaces. *Phys. Rev. B* **49**, 16721–16727 (1994).
40. Diebold, U. The surface science of titanium dioxide. *Surf. Sci. Rep.* **48**, 53–229 (2002).
41. Mondal, D. et al. Atomically-smooth single-crystalline VO₂(101) thin films with sharp metal-insulator transition. *J. Appl. Phys.* **126**, 215302 (2019).
42. Kittiwatanakul, S. & Al, E. A near-field study of VO₂/(100)TiO₂ film and its crack-induced strain relief. *Appl. Phys. Lett.* **121**, 021902 (2022).
43. Kawatani, K., Takami, H., Kanki, T. & Tanaka, H. Metal-insulator transition with multiple micro-scaled avalanches in VO₂ thin film on TiO₂ (001) substrates. *Appl. Phys. Lett.* **100**, 173112 (2012).
44. Krispeneit, J. O. et al. The morphology of terraces, facets, and cracks. *Scientific Reports* **10**, 22374 (2020).
45. Panaccione, G. et al. Advanced photoelectric effect experiment beamline at Elettra: A surface science laboratory coupled with Synchrotron Radiation. *Rev. Sci. Instrum.* **80**, 043105 (2009).
46. Stöhr, J. Principles, Techniques, and Instrumentation of NEXAFS, NEXAFS Spectroscopy, Springer Series in Surface Sciences, vol 25, 114–161, (1992).
47. Aetukuri, N. B. et al. Control of the metal-insulator transition in vanadium dioxide by modifying orbital occupancy. *Nat. Phys.* **9**, 661–666 (2013).
48. Haverkort, M. W. et al. Orbital-assisted metal-insulator transition in VO₂. *Phys. Rev. Lett.* **95**, 196404 (2005).
49. Liang, Y. G. et al. Tuning the hysteresis of a metal-insulator transition via lattice compatibility. *Nature Communications* **11**, 3539 (2020).
50. Polewczyk, V. et al. Chemical, structural and electronic properties of ultrathin V₂O₃ films on Al₂O₃ substrate: Implications in Mott-like transitions. *Appl. Surf. Sci.* **610**, 155462 (2023).
51. Polewczyk, V. et al. Tuning the magnetic properties of V₂O₃/CoFeB heterostructures across the V₂O₃ structural transition. *Phys. Rev. Mater.* **5**, 34413 (2021).
52. D'Elia, A. et al. A Strain Induced Orbital Dynamics Across the Metal Insulator Transition in Thin VO₂/TiO₂ (001) Films. *J. Supercond. Nov. Magn.* **33**, 2383–2388 (2020).
53. D'Elia, A. et al. Strain mediated Filling Control nature of the Metal-Insulator Transition of VO₂ and electron correlation effects in nanostructured films. *Appl. Surf. Sci.* **540**, 148341 (2021).
54. Laverock, J. et al. Photoemission evidence for crossover from Peierls-like to Mott-like transition in highly strained VO₂. *Phys. Rev. B Condens Matter Mater. Phys.* **86**, 195124 (2012).
55. Eguchi, R. et al. Photoemission evidence for a Mott-Hubbard metal-insulator transition in VO₂. *Phys. Rev. B Condens Matter Mater. Phys.* **78**, 075115 (2008).
56. D'Elia, A. et al. Detection of Spin Polarized Band in VO₂/TiO₂(001) Strained Films via Orbital Selective Constant Initial State Spectroscopy. *Condens. Matter.* **5**, 72 (2020).
57. Marcelli, A. et al. Nanoscale Phase Separation and Lattice Complexity in VO₂: The Metal-Insulator Transition Investigated by XANES via Auger Electron Yield at the Vanadium L23-Edge and Resonant Photoemission. *Condens. Matter.* **2**, 38 (2017).
58. Lee, W. C. et al. Cooperative effects of strain and electron correlation in epitaxial VO₂ and NbO₂. *J. Appl. Phys.* **125**, 082539 (2019).
59. Mossaneh, R. J. O. & Abbate, M. Cluster model calculations with nonlocal screening channels of metallic and insulating VO₂. *Phys. Rev. B Condens Matter Mater. Phys.* **74**, 125112 (2006).
60. Demeter, M., Neumann, M. & Reichelt, W. Mixed-valence vanadium oxides studied by XPS. *Surf. Sci.* **454**, 41–44 (2000).
61. Dowben, P. A. Metallicity of thin films and overlayers. *Surf. Sci. Rep.* **40**, 151–247 (2000).
62. McIlroy, D. et al. Comparison of the temperature-dependent electronic structure of the perovskites. *Phys. Rev. B Condens Matter Mater. Phys.* **54**, 17438–17451 (1996).
63. Li, D., Zhang, J., Lee, S. & Dowben, P. A. Evidence for the formation of metallic mercury overlayers on Si(111). *Phys. Rev. B* **45**, 11876–11884 (1992).
64. Pergament, A. & Stefanovich, G. Insulator-to-metal transition in vanadium sesquioxide: does the Mott criterion work in this case? *Phase Transit* **85**, 185–194 (2012).
65. Kim, R., Wang, X. & Lundstrom, M. *Notes on Fermi-Dirac Integrals*, 4th ed. arXiv, 0811.0116, (2008).
66. Jonsson, V. et al. Photoelectron dispersion in metallic and insulating VO₂ thin films. *Phys. Rev. Res* **3**, 33286 (2021).
67. Lazarovits, B., Kim, K., Haule, K. & Kotliar, G. Effects of strain on the electronic structure of VO₂. *Phys. Rev. B* **81**, 115117 (2010).
68. Mukherjee, S. et al. Tuning a strain-induced orbital selective Mott transition in epitaxial VO₂. *Phys. Rev. B* **93**, 241110(R) (2016).